

See discussions, stats, and author profiles for this publication at: <https://www.researchgate.net/publication/46094207>

STAT3 Silencing in Dendritic Cells by siRNA Polyplexes Encapsulated in PLGA Nanoparticles for the Modulation of Anticancer Immune Response

ARTICLE *in* MOLECULAR PHARMACEUTICS · SEPTEMBER 2010

Impact Factor: 4.38 · DOI: 10.1021/mp100067u · Source: PubMed

CITATIONS

32

READS

86

7 AUTHORS, INCLUDING:



Azita Haddadi

University of Saskatchewan

67 PUBLICATIONS 648 CITATIONS

[SEE PROFILE](#)



Ayman O S El-Kadi

University of Alberta

163 PUBLICATIONS 2,663 CITATIONS

[SEE PROFILE](#)



Afsaneh Lavasanifar

University of Alberta

138 PUBLICATIONS 4,721 CITATIONS

[SEE PROFILE](#)

STAT3 Silencing in Dendritic Cells by siRNA Polyplexes Encapsulated in PLGA Nanoparticles for the Modulation of Anticancer Immune Response

Aws Alshamsan,^{†,‡} Azita Haddadi,^{†,¶} Samar Hamdy,[†] John Samuel,^{†,§} Ayman O. S. El-Kadi,[†] Hasan Uludağ,^{†,||,⊥} and Afsaneh Lavasanifar^{*,†,||}

Faculty of Pharmacy and Pharmaceutical Sciences, University of Alberta, Canada,

Department of Pharmaceutics, College of Pharmacy, King Saud University,

Riyadh, Saudi Arabia, Department of Chemical and Material Engineering, Faculty of Engineering, University of Alberta, Canada, and Department of Biomedical Engineering,

Faculty of Medicine and Dentistry, University of Alberta, Canada

Received March 13, 2010; Revised Manuscript Received August 28, 2010; Accepted August 30, 2010

Abstract: In dendritic cells (DCs), the induction of signal transducer and activator of transcription 3 (STAT3) by tumor-derived factors (TDFs) renders DCs tolerogenic and suppresses their antitumor activity. Therefore, silencing STAT3 in DCs is beneficial for cancer immunotherapy. We have shown that STAT3 knockdown in B16 murine melanoma by siRNA polyplexes of polyethylenimine (PEI) or its stearic acid derivative (PEI-StA) induces B16 cell death *in vitro* and *in vivo*. Here, we investigated the physical encapsulation of siRNA/PEI and PEI-StA polyplexes in poly(D,L-lactic-co-glycolic acid) (PLGA) nanoparticles (NPs) for STAT3 knockdown in DCs. PLGA NPs containing siRNA polyplexes of PEI (PLGA-P) and PEI-StA (PLGA-PS) had an average diameter of ~350 to 390 nm and a zeta potential of ~−13 to −19 mV, respectively. The encapsulation efficiency (E.E.) of siRNA in PLGA-P and PLGA-PS was 26% and 43%, respectively. In both NP types, siRNA release followed a triphasic pattern, but it was faster in PLGA-PS. Our uptake study by fluorescence microscopy confirmed DC uptake and endosomal localization of both NP types. After exposure to B16.F10 conditioned medium, DCs showed high STAT3 and low CD86 expression indicating impaired function. STAT3 silencing by PLGA-P and PLGA-PS of STAT3 siRNA restored DC maturation and functionality as evidenced by the upregulation of CD86 expression, high secretion of TNF- α , and significant allogenic T cell proliferation. Moreover, encapsulation in PLGA NPs significantly reduced PEI-associated toxicity on DCs. We propose this formulation as a strategy for targeted siRNA delivery to DCs. The potential of this approach is not limited to STAT3 downregulation in DCs but can be used to target the expression of other proteins as well. Moreover, it can be combined with other means for cancer immunotherapy like cancer vaccine strategies.

Keywords: Dendritic cells; STAT3, siRNA; polyethylenimine; PLGA, cancer immunotherapy

1. Introduction

Dendritic cells (DCs) are professional antigen presenting cells (APCs) that serve as sentinels against internal and

external pathogens in most peripheral tissues.^{1–3} Typically, when immature DCs (imDCs) encounter antigens, they get

[†] Department of Chemical and Material Engineering, Faculty of Engineering, University of Alberta.

[‡] Department of Biomedical Engineering, Faculty of Medicine and Dentistry, University of Alberta.

[¶] Current address: College of Pharmacy and Nutrition, University of Saskatchewan, Saskatoon, Saskatchewan, Canada.

(1) Banchereau, J.; Steinman, R. M. Dendritic cells and the control of immunity. *Nature* **1998**, 392 (6673), 245–52.

(2) Stockwin, L. H.; McGonagle, D.; Martin, I. G.; Blair, G. E. Dendritic cells: immunological sentinels with a central role in health and disease. *Immunol. Cell Biol.* **2000**, 78 (2), 91–102.

* Corresponding author. Mailing address: # 4119 Dent/Pharm Centre, University of Alberta, Edmonton, AB, Canada T6G 2N8. Tel: (780) 492-2742. Fax: (780) 492-1217. E-mail: alavasanifar@pharmacy.ualberta.ca.

[†] Faculty of Pharmacy and Pharmaceutical Sciences, University of Alberta.

[‡] King Saud University.

[§] This manuscript is dedicated to the memory of Dr. John Samuel who initiated a research program encompassing this study.

activated and transformed into mature DCs (mDCs) that express high levels of major histocompatibility complex (MHC) class I and class II, costimulatory molecules, as well as proinflammatory cytokines.^{4,5} These mDCs migrate to secondary lymphoid organs where they activate naive mature CD4⁺ and CD8⁺ T cells.^{6,7} However, in tumor microenvironment, DCs cannot exert their proper function due to the state of immune tolerance enforced by tumor milieu.⁸ One mechanism by which tumors abrogate DC function is through the constitutive activation of signal transducer and activator of transcription 3 (STAT3).⁹

STAT3 is a transcription factor that becomes activated in response to cytokine and growth factor receptor stimulation.¹⁰ For activation, STAT3 monomers get phosphorylated on critical tyrosine residues (Y⁷⁰⁵) by Janus kinases (JAKs). Thereafter, monomers of phosphorylated-STAT3 (p-STAT3) dimerize through reciprocal phosphotyrosine-SH2 interaction and translocate to the nucleus where they bind to STAT-specific sites on the promoter region of the target genes.¹⁰ In tumor cells, many tumor-derived factors (TDFs) induce the transcriptional activity of p-STAT3 such as vascular endothelial growth factor (VEGF), interleukin-6 (IL-6), and IL-10.¹¹ The secretion of these TDFs in tumor milieu leads to further induction of p-STAT3 in several tumor-exposed immune cells including DCs.¹¹ This hyperactive STAT3 forces DCs to remain immature and malfunctioned expressing low levels of MHC class I/II, costimulatory molecules, and proinflammatory cytokines.^{12,13} Therefore, DCs lose their ability to polarize T cells toward T helper type 1 (Th1) and

cytotoxic T lymphocyte (CTL) response, which is needed for antitumoral immunity.¹⁴ In fact, numerous studies strongly indicated the negative-regulatory role of JAK/STAT3 pathway on DC maturation, which has been systematically evidenced *in vivo*.^{15–17} As a result, the antitumor activity mediated by DCs gets profoundly harnessed.^{9,11,18–21} Hence, the disruption of tumor-induced hyperactive p-STAT3 in DCs is considered as an attractive strategy for cancer immunotherapy.

Several modalities have been employed to study antitumor immune responses following STAT3 inhibition in DCs. Pioneer studies focused on the inhibition of JAKs as a mean for STAT3 activity disruption. In fact, targeted disruption of STAT3 signaling in APCs using AG490, a known inhibitor of JAK1 and JAK2, resulted in the priming of antigen-specific CD4⁺ T cells in response to an otherwise tolerogenic stimulus *in vivo*.¹⁶ Consistently, the work of Gabrilovich and colleagues on the JAK2/STAT3 inhibitor JSI-124 (cucurbitacin I) demonstrated a dramatic activation of imDCs generated in the presence of TDFs as well as in control medium.¹⁷ The outcomes from STAT3 disruption data in DCs support the use of this approach for therapeutic applications. However, due to the incomplete understanding of the mechanism of inhibition by which these agents act, as well as the apparently generalized upstream action and the associated nonspecific toxicities of these pharmacological inhibitors, clinical applications of AG490 or JSI-124 were not possible.²² Therefore, the need is imminent for specific STAT3 inhibition strategies.

Recently, RNA interference (RNAi) emerged as a specific and effective modality to downregulate protein expression

-
- (3) Shortman, K.; Liu, Y. J. Mouse and human dendritic cell subtypes. *Nat. Rev. Immunol.* **2002**, 2 (3), 151–61.
 - (4) Steinman, R. M.; Banchereau, J. Taking dendritic cells into medicine. *Nature* **2007**, 449 (7161), 419–26.
 - (5) Steinman, R. M. Lasker Basic Medical Research Award. Dendritic cells: versatile controllers of the immune system. *Nat. Med.* **2007**, 13 (10), 1155–9.
 - (6) Kalinski, P.; Hilkens, C. M.; Wierenga, E. A.; Kapsenberg, M. L. T-cell priming by type-1 and type-2 polarized dendritic cells: the concept of a third signal. *Immunol. Today* **1999**, 20 (12), 561–7.
 - (7) Trombetta, E. S.; Mellman, I. Cell biology of antigen processing *in vitro* and *in vivo*. *Annu. Rev. Immunol.* **2005**, 23, 975–1028.
 - (8) Yang, L.; Carbone, D. P. Tumor-host immune interactions and dendritic cell dysfunction. *Adv. Cancer Res.* **2004**, 92, 13–27.
 - (9) Gabrilovich, D. Mechanisms and functional significance of tumour-induced dendritic-cell defects. *Nat. Rev. Immunol.* **2004**, 4 (12), 941–52.
 - (10) Turkson, J.; Jove, R. STAT proteins: novel molecular targets for cancer drug discovery. *Oncogene* **2000**, 19 (56), 6613–26.
 - (11) Yu, H.; Kortylewski, M.; Pardoll, D. Crosstalk between cancer and immune cells: role of STAT3 in the tumour microenvironment. *Nat. Rev. Immunol.* **2007**, 7 (1), 41–51.
 - (12) Gabrilovich, D. I.; Chen, H. L.; Girgis, K. R.; Cunningham, H. T.; Meny, G. M.; Nadaf, S.; Kavanaugh, D.; Carbone, D. P. Production of vascular endothelial growth factor by human tumors inhibits the functional maturation of dendritic cells. *Nat. Med.* **1996**, 2 (10), 1096–103.
 - (13) Sumimoto, H.; Imabayashi, F.; Iwata, T.; Kawakami, Y. The BRAF-MAPK signaling pathway is essential for cancer-immune evasion in human melanoma cells. *J. Exp. Med.* **2006**, 203 (7), 1651–6.
 - (14) Kennedy, R.; Celis, E. Multiple roles for CD4⁺ T cells in anti-tumor immune responses. *Immunol. Rev.* **2008**, 222, 129–44.
 - (15) Park, S. J.; Nakagawa, T.; Kitamura, H.; Atsumi, T.; Kamon, H.; Sawa, S.; Kamimura, D.; Ueda, N.; Iwakura, Y.; Ishihara, K.; Murakami, M.; Hirano, T. IL-6 regulates *in vivo* dendritic cell differentiation through STAT3 activation. *J. Immunol.* **2004**, 173 (6), 3844–54.
 - (16) Cheng, F.; Wang, H. W.; Cuenca, A.; Huang, M.; Ghansah, T.; Brayer, J.; Kerr, W. G.; Takeda, K.; Akira, S.; Schoenberger, S. P.; Yu, H.; Jove, R.; Sotomayor, E. M. A critical role for Stat3 signaling in immune tolerance. *Immunity* **2003**, 19 (3), 425–36.
 - (17) Nefedova, Y.; Cheng, P.; Gilkes, D.; Blaskovich, M.; Beg, A. A.; Sefti, S. M.; Gabrilovich, D. I. Activation of dendritic cells via inhibition of Jak2/STAT3 signaling. *J. Immunol.* **2005**, 175 (7), 4338–46.
 - (18) Imada, K.; Leonard, W. J. The Jak-STAT pathway. *Mol. Immunol.* **2000**, 37 (1–2), 1–11.
 - (19) Kortylewski, M.; Yu, H. Role of Stat3 in suppressing anti-tumor immunity. *Curr. Opin. Immunol.* **2008**, 20 (2), 228–33.
 - (20) Vicari, A. P.; Caux, C.; Trinchieri, G. Tumour escape from immune surveillance through dendritic cell inactivation. *Semin. Cancer Biol.* **2002**, 12 (1), 33–42.
 - (21) Zou, W. Immunosuppressive networks in the tumour environment and their therapeutic relevance. *Nat. Rev. Cancer* **2005**, 5 (4), 263–74.
 - (22) Yue, P.; Turkson, J. Targeting STAT3 in cancer: how successful are we. *Expert Opin. Invest. Drugs* **2009**, 18 (1), 45–56.

at the mRNA level.²³ This technology is based on introducing a small interfering RNA (siRNA) in the cytoplasm where it integrates into RNA-induced silencing complex (RISC) that cleaves the mRNA of interest specifically.²⁴ However, due to low biological stability, poor cell permeability, and unfavorable pharmacokinetic and biodistribution profile, the progress of siRNA from bench to bedside was significantly hindered.²⁵ Hence, it is important to develop an optimum siRNA delivery strategy.²⁶ In this regard, we have previously developed siRNA delivery systems based on lipid modification of polyethylenimine (PEI).²⁷ We have shown that attachment of stearic acid molecules on PEI backbone (PEI-StA) enhances the protective effect of PEI against degradation of complexed siRNA in serum.²⁷ Moreover, the anti-STAT3 activity of the PEI and PEI-StA polyplexes was proven in B16 melanoma cells *in vitro* and *in vivo* where PEI-StA, in particular, enhanced the silencing potency of STAT3 siRNA and promoted its anticancer activity.²⁸ Moreover, STAT3 knockdown in B16 tumor by siRNA/PEI-StA complexes induced a bystander antitumor immune response evidenced by high infiltration and activation levels of DCs, CD4⁺, CD8⁺ and NKT cells into tumor mass. However, knockdown of STAT3 in DC directly with anti-STAT3 siRNA has not been investigated. In this study we evaluate this approach by designing a delivery system based on physical encapsulation of siRNA/PEI or siRNA/PEI-StA complexes in poly(D,L-lactic-co-glycolic acid) (PLGA) nanoparticles (NPs) (Figure 1). The incorporation of siRNA polyplexes into PLGA NPs improves the toxicity profile of PEI and enhances cellular uptake.²⁹ To our knowledge, for the first time we provide evidence that PLGA NPs of STAT3 siRNA could restore DC maturation and functionality after exposure to tumor factors while masking the PEI-associated toxicity.

- (23) Cejka, D.; Losert, D.; Wacheck, V. Short interfering RNA (siRNA): tool or therapeutic. *Clin. Sci. (London)* **2006**, *110* (1), 47–58.
- (24) Kawasaki, H.; Taira, K.; Morris, K. V. siRNA induced transcriptional gene silencing in mammalian cells. *Cell Cycle* **2005**, *4* (3), 442–8.
- (25) Hede, K. Blocking cancer with RNA interference moves toward the clinic. *J. Natl. Cancer Inst.* **2005**, *97* (9), 626–8.
- (26) Thomas, M.; Lu, J. J.; Chen, J.; Klibanov, A. M. Non-viral siRNA delivery to the lung. *Adv. Drug Delivery Rev.* **2007**, *59* (2–3), 124–33.
- (27) Alshamsan, A.; Haddadi, A.; Incani, V.; Samuel, J.; Lavasanifar, A.; Uludag, H. Formulation and delivery of siRNA by oleic acid and stearic acid modified polyethylenimine. *Mol. Pharmaceutics* **2009**, *6* (1), 121–33.
- (28) Alshamsan, A.; Hamdy, S.; Samuel, J.; El-Kadi, A. O.; Lavasanifar, A.; Uludag, H. The induction of tumor apoptosis in B16 melanoma following STAT3 siRNA delivery with a lipid-substituted polyethylenimine. *Biomaterials* **2010**, *31* (6), 1420–8.
- (29) Zhang, X. Q.; Intra, J.; Salem, A. K. Comparative study of poly (lactic-co-glycolic acid)-poly ethyleneimine-plasmid DNA microparticles prepared using double emulsion methods. *J. Microencapsulation* **2008**, *25* (1), 1–12.

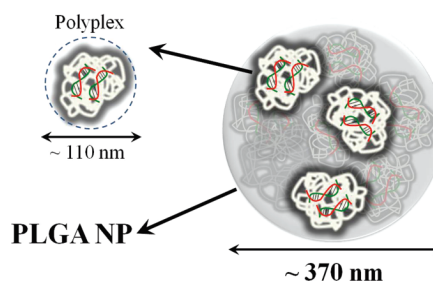


Figure 1. Schematic diagram showing components of PLGA-P or PLGA-PS nanoparticulate formulation with relative sizes to the polyplexes counterparts.

2. Materials and Methods

2.1. Materials. Branched PEI (25 kDa), triethylamine (TEA), 3-(4,5-dimethylthiazol-2-yl)-2,5-diphenyltetrazolium bromide (MTT), dimethyl sulfoxide (DMSO), and stearoyl chloride (98.5%) were obtained from Sigma-Aldrich (St. Louis, MO). Polyvinyl alcohol (PVA) was purchased from Sigma-Aldrich (St. Louis, MO), carboxylic acid terminated PLGA polymers (monomer ratio 50:50, MW ~7 kDa) was purchased from Absorbable Polymers International (Pelham, AL). Anhydrous ethyl ether and dichloromethane (DCM) were purchased from Fisher Scientific (Fairlawn, NJ). Fetal Bovine Serum (FBS) was obtained from HyClone (Logan, UT). Dulbecco's modified Eagle's medium (DMEM), RPMI-1640, L-glutamine, and gentamicin were purchased from Gibco-BRL (Burlington, ON, Canada). Mouse TNF- α ELISA kit was purchased from e-Biosciences (San Diego, CA). Sequence-specific siRNA targeting murine STAT3 mRNA was purchased from Ambion (Austin, TX) (sense, 5'-GGACGACUUUGAUUCAACtt-3'; antisense, 5'-GUUGAAAUCAAAGUCGUCCtgc-3'). The scrambled Silencer Negative Control #1 siRNA (Catalog #AM4635) and Silencer FAM labeled Negative Control #1 siRNA (Catalog #AM4620) were purchased from Ambion (Austin, TX). LysoTracker Red DND-99 and ProLong Gold Antifade with DAPI were purchased from Invitrogen (Burlington, ON, Canada). Anti-mouse CD86 (PE labeled) mAb was purchased from BD Biosciences (Mississauga, ON, Canada). EasySep Negative Selection kit for T cells isolation was purchased from Stemcell Technologies (Vancouver, BC, Canada). Anti-phosphotyrosine (Y⁷⁰⁵) STAT3 monoclonal antibody, anti-STAT3 antibody and anti-actin antibody (I-19) were purchased from Santa Cruz Biotechnology (Santa Cruz, CA). ECL Plus detection kit was purchased from GE Healthcare Life Sciences (Piscataway, NJ).

2.2. Preparation of Primary DC Culture. Primary DC culture was generated from bone marrow precursor of C57BL/6 mice femurs and propagated in complete RPMI-1640 in presence of GM-CSF as previously described.³⁰ The purity of the DC population on day 7 was found to be

- (30) Lutz, M. B.; Kukutsch, N.; Ogilvie, A. L.; Rossner, S.; Koch, F.; Romani, N.; Schuler, G. An advanced culture method for generating large quantities of highly pure dendritic cells from mouse bone marrow. *J. Immunol. Methods* **1999**, *223* (1), 77–92.

between 70 and 75% based on the expression of CD11c on the semiadherent and nonadherent cell populations. To increase DC purity, semiadherent and nonadherent cells were isolated from primary culture on day 6 by thorough suspension in growth medium. Cells were centrifuged and resuspended in fresh complete RPMI-1640 in the presence of GM-CSF and then transferred to new cell culture plates 24 h prior to any manipulation. After this process, 95% of cells were confirmed to be positive for CD11c.

2.3. Preparation of PLGA NPs Containing siRNA Polyplexes. PEI-StA was prepared by N-acylation of PEI with stearoyl chloride and characterized as described in ref 31. Then, in sterile eppendorf tubes, 12.5 μ g of siRNA was added to equal amount of PEI or PEI-StA in 50 μ L of PBS and incubated for 30 min at 37 °C as previously described.²⁷ Thereafter, the formed complexes were encapsulated into PLGA NPs by double-emulsion solvent evaporation method regularly used in our lab. In brief, a primary w/o emulsion is formed by emulsification of the first aqueous phase (PEI or PEI-StA polyplexes in 50 μ L of PBS) with the organic phase (25 mg of PLGA in 300 μ L of DCM) using a microtip probe sonicator (model XL2010, Heat Systems, Farmingdale, NY). The primary emulsion is further emulsified with a secondary aqueous phase (1 mL of 5% PVA in PBS) to form a secondary w/o/w emulsion. The resulting emulsion is transferred dropwise to stirring 4 mL of double-deionized water to allow the removal of DCM by evaporation. After 3 h, the NP suspension is washed three times at 4 °C (35000g, 15 min) and freeze-dried.

2.4. Characterization of PLGA-P and PLGA-PS.

2.4.1. Surface Morphology, Particle Size, and Surface Charge Analysis. From freeze-dried stocks, PLGA-P or PLGA-PS suspensions of 1 mg/mL in water were prepared. Thereafter, aliquots of PLGA-P or PLGA-PS suspensions were aspirated and mounted on specimen stubs and sputter coated with Au/Pd in Hummer 6.2 sputter coater. After 24 h, samples were visualized by scanning electron microscope XL30 (FEI Company, Hillsboro, OR, Canada) and SEM images were taken. Other aliquots were used for size and surface charge analysis by dynamic light scattering (DLS) and zeta potential analysis, respectively, of 3 serial measurements using Zetasizer 3000 (Malvern, U.K.).

2.4.2. Determination of siRNA Content. Encapsulation efficiency (E.E.) and loading of siRNA in PLGA-P and PLGA-PS NPs were calculated by fluorescence spectroscopy and confirmed by gel retardation assay. FAM-labeled siRNA was complexed with PEI or PEI-StA and then encapsulated in PLGA NPs as described above. Serial dilution of each sample was prepared and read at ($\lambda_{ex} = 484$ nm and $\lambda_{em} = 535$ nm) in a Baxter 96-well plate fluorescence reader

(Chicago, IL). Blank PLGA NPs spiked with known serial concentrations of siRNA-polyplexes were used as calibration curve.

For gel retardation assay, PLGA-P and PLGA-PS were dissolved in chloroform. The solvent was evaporated under nitrogen, and precipitants were suspended in RNase-Free water. Supernatant (containing siRNA + PEI or PEI-StA polyplexes) was incubated with 50 μ g of heparin at 37 °C for 1 h to ensure that all siRNA is released in free form, as previously described in ref 27. The samples were then loaded onto 2% agarose gel containing 0.2% mg/mL EtBr, and electrophoresis was performed under previously described conditions.²⁷ The resulting gel was photographed under UV illumination. The pictures were digitized and analyzed with ImageJ software (W. Rasband (2005) National Institutes of Health, Bethesda, MD, <http://rsb.info.nih.gov/ij>) to determine the mean density of siRNA band. To determine the recovery of the extraction process, known amount of siRNA/polyplexes and empty PLGA NPs were added into chloroform, and the extraction procedure was performed as described above. Thereafter, E.E. % and siRNA loading (w/w) were calculated using the following equations:

$$\text{E.E. \%} = \frac{\text{amount of loaded siRNA in } \mu\text{g}}{\text{amount of total siRNA used in } \mu\text{g}} \times 100$$

$$\text{siRNA loading (w/w)} = \frac{\text{amount of loaded siRNA in } \mu\text{g}}{\text{amount of PLGA in mg}}$$

2.4.3. In Vitro Release Study. Aliquots of 5 mg/mL of the suspended PLGA-P and PLGA-PS in PBS were placed in a 37 °C gently shaking water bath. At designated time intervals, a set of triplicate samples was removed, and the supernatant was separated from the particles by centrifugation. Fluorescence spectroscopy was used to determine siRNA concentration as mentioned earlier. To determine the remaining siRNA in the precipitated portion, pellets were dissolved and run on agarose gel as described above.

2.5. Cytotoxicity Studies. DCs on day 7 were transferred to 6-well plates at cell density of 2×10^5 cells per well. Then, cells were subjected to scrambled siRNA treatment in PEI complexes, PEI-StA complexes, PLGA-P, or PLGA-PS for 24 h at 37 °C. The treatment dose was calculated based on 10 μ g/mL PEI or PEI-StA concentration in culture media. After designated treatments, cells were washed with PBS. Then, 1 mL of Trypan Blue in medium (1:1 ratio) was added, and Trypan Blue exclusion was detected by Axio Observer Z1 Inverted Microscope (Carl Zeiss Canada Ltd., Toronto, ON, Canada) and visualized with Axio Vision 4.8 software.

To determine cell viability as a function of polyplex concentrations, MTT assay was carried out. Day 7 DCs were transferred to 96-well plate at cell density of 5,000 cells per well. Then, cells were incubated with PEI complexes, PEI-StA complexes, PLGA-P, or PLGA-PS for 24 h at 37 °C. Thereafter, 100 μ L of MTT solution in culture medium (0.5 mg/mL) was added to each well for 2 h. The formed formazan crystals were dissolved by adding 200 μ L of DMSO to each well and kept under gentle shaking for 30 min. Optical density was measured

(31) Incani, V.; Tunis, E.; Clements, B. A.; Olson, C.; Kucharski, C.; Lavasanifar, A.; Uludag, H. Palmitic acid substitution on cationic polymers for effective delivery of plasmid DNA to bone marrow stromal cells. *J. Biomed. Mater. Res., Part A* **2007**, 81 (2), 493–504.

at 550 nm using a microplate reader (Powerwave with KC Junior software; Bio-Tek, Winooski, VT). The results were converted into % viability by using the absorbance from untreated sample as a reference (100%), and expressing the absorbances obtained from the treatment groups as a percentage of the reference value.

2.6. Uptake of PLGA-P and PLGA-PS by DCs. DC uptake of PLGA-P and PLGA-PS was determined by fluorescence microscopy. Day 7 DCs were transferred to 24-well plates and grown on coverslips for 24 h. Then, DCs were pulsed for 6 h at 37 °C with PLGA-P and PLGA-PS encapsulating FAM-labeled scrambled siRNA (100 nM). Then, LysoTracker Red DND-99 at a concentration of 100 nM was added for 30 min. The cells were then washed three times with PBS and fixed with 2% paraformaldehyde solution in PBS for 10 min. Then, ProLong Gold Antifade with DAPI was mounted to prevent photobleaching as well as to stain the nucleus. Samples were then visualized under with Axio Observer Inverted Microscope (Carl Zeiss Canada Ltd., Toronto, ON, Canada).

2.7. Treatment of Malfunctioned DCs. Malfunctioned DCs at day 7 were generated by exposure to tumor-conditioned media from B16.F10 melanoma culture (B16-CM) for 24 h as previously described in ref 32. In brief, murine B16.F10 cells were grown and propagated in DMEM medium supplemented with 10% FBS at 37 °C and 5% CO₂. After confluence, B16 cells were incubated with serum-free medium for 24 h. Thereafter, conditioned medium was added to a primary DC culture reaching a final B16-CM concentration of 50%. FBS was then supplemented to 10% final concentration in culture. Then, DCs were pulsed with anti-STAT3 PLGA-P and PLGA-PS for 48 h. As controls, DCs treated with naked anti-STAT3 siRNA or PLGA-P and PLGA-PS of scrambled siRNA (PLGA-P-sc) and (PLGA-PS-sc) were used. Thereafter, STAT3 activation level in DCs was determined by Western blot, phenotypic maturation was assessed by analyzing CD86 expression by fluorescence activated cell sorting (FACS), TNF-α secretion was determined by ELISA, and DC alloreactivity was assessed by mixed lymphocytes reaction (MLR).

2.7.1. Western Blot. After designated treatments, DCs were collected and washed twice with ice-cold PBS and then lysed in a buffer containing 30 mM HEPES (pH 7.5), 2 mM Na₃VO₄, 25 mM NaF, 2 mM EGTA, 2% Nonidet P-40, 1:100 protease inhibitor cocktails, 0.5 mM DTT and 6.4 mg/mL phosphatase substrate 4-nitrophenyl phosphate. Cell lysates were centrifuged for 20 s at 16000g (eppendorf centrifuge 5415C). Thereafter, NaCl was added to samples to a final concentration of 420 mM, cell lysates were centrifuged for 20 min at 16000g, supernatant was transferred to new tubes and pellets were discarded. Total protein extract was determined by Micro BCA Protein Assay kit. Equal amounts of protein (20 µg) were loaded on an 8%

SDS-PAGE gel. Proteins were then transferred into PVDF membrane and were probed with anti-phosphotyrosine (Y⁷⁰⁵) STAT3 monoclonal antibody (1:500). Stripped membranes were probed with polyclonal anti-STAT3 antibody (1:1000) or anti-actin antibody (I-19) (1:1000). Membranes were developed using ECL Plus detection kit. The optical intensity of the p-STAT3 band was quantified and normalized to actin protein band using ImageJ software (W. Rasband (2005) National Institutes of Health, Bethesda, MD, <http://rsb.info.nih.gov/ij>).

2.7.2. FACS Analysis. For phenotypic maturation studies, 1 × 10⁵ DC primary cultures were washed with PBS and suspended in FACS buffer. Then, cells were incubated with CD86 mAbs or corresponding isotype controls and kept at 4 °C for 30 min. After that, cells were washed 3 times with FACS buffer to remove excess mAbs and all samples were finally acquired on a Becton-Dickinson FACSort and analyzed by Cell-Quest software.

2.7.3. ELISA Assay. After designated treatments, supernatants of DC cultures were collected after centrifugation at 10000g for 5 min (eppendorf centrifuge 5415C). Then, several dilutions of supernatants were loaded in a 96-well plate precoated with anti-TNF-α mAb. Sandwich ELISA was performed using mouse TNF-α ELISA kit according the manufacturer's directions. The resulting color, proportional to TNF-α concentration, was read using a microplate reader (Powerwave with KC Junior software; Bio-Tek, Winooski, VT) at OD of 450 nm with reference set at 570 nm. Concentration was calculated from standard curve of authentic TNF-α sample provided by the manufacturer.

2.7.4. Mixed Lymphocyte Reaction. T cells were obtained from spleen of Balb/c mice Jackson Laboratory (Bar Harbor, ME). Spleen was crushed between two slides, and T cells were purified using EasySep Negative Selection kit according to the manufacturer's instructions. Purified T cells were cocultured in flat-bottomed 96-well plates with irradiated DCs in a ratio of 2:1 at 37 °C and 5% CO₂. Thereafter, [³H]thymidine was added during the last 18 h of a 3 day coculture and the T-cell proliferation was measured by [³H]thymidine incorporation in counts per minute.

2.8. Data Analysis. The data were analyzed for statistical significance ($p < 0.05$) by one-way ANOVA; post-hoc Scheffé's test was conducted to determine level of significance (SPSS for Windows, Version 16.0).

3. Results

3.1. Characterization of PLGA-P and PLGA-PS. Surface morphology, size distribution, and zeta potential analysis for PLGA-P and PLGA-PS are shown in Figure 2. Evaluation of NP surface morphology by scanning electron microscopy (SEM) showed that PLGA-P and PLGA-PS form spherical structures with smooth surfaces. Size determination by DLS indicates that both PLGA-P and PLGA-PS formed uniform populations evidenced by the Gaussian distribution of the hydrodynamic diameter histograms. PLGA-PS was slightly, but not significantly, larger than PLGA-P (the average hydrodynamic diameter for PLGA-P and PLGA-PS was 351

(32) Alshamsan, A.; Hamdy, S.; Das, S.; Lavasanifar, A.; Samuel, J.; El-Kadi, A. O. Bone Marrow Derived Dendritic Cells are More Suitable than Dendritic Cell Line DC2.4 to Study Tumor-Mediated Suppression of DC Maturation through STAT3 Hyperactivation. *J. Pharm. Pharm. Sci.* **2010**, 13 (1), 21–26.

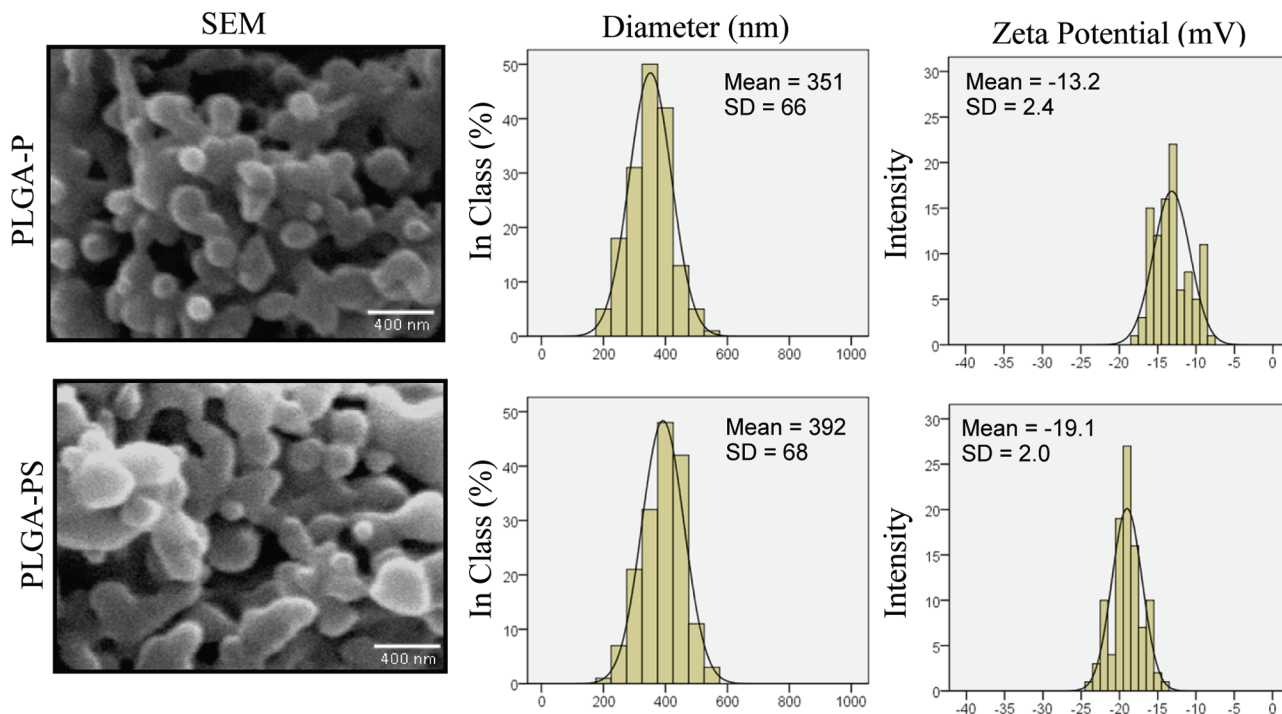


Figure 2. Characterization of PLGA-P and PLGA-PS NPs. SEM images (left panels) of dried samples showing spherical structures of smooth surfaces. Bar scale is 400 nm. Binning charts represent Gaussian distribution histogram of hydrodynamic diameter of PLGA-P and PLGA-PS (middle panels). Mean \pm SD for each sample is presented in the upper corner of each panel. Mean hydrodynamic diameters of all NPs did not show any significant difference from each other. Gaussian distribution demonstrated no skewness indicating the uniformity of sample population. The data is representative of 10 reading cycles for 3 independent measurements. Binning chart histograms for zeta potential distribution (mV) (right panels) demonstrated no skewness indicating the uniformity of sample population. Mean \pm SD for each sample is presented in the upper corner of each panel. The data is representative of 10 reading cycles for 3 independent measurements.

Table 1. siRNA E.E. and Loading in PLGA-based NPs

formulation	E.E. (%)	loading ($\mu\text{g}/\text{mg}$) ^a
PLGA-P	26.31 \pm 5.96	2.2 \pm 0.4
PLGA-PS	43.98 \pm 6.07 ^a	3.8 \pm 0.3 ^b

^a siRNA loading per 1 mg of PLGA. ^b Statistical significance at $p < 0.05$.

and 392 nm, respectively). Moreover, surface charge analysis indicated that PLGA-P and PLGA-PS displayed comparable negative surface charges reaching ~ -13 and -19 mV, respectively. The difference was not statistically significant.

Moreover, siRNA encapsulation efficiency in PLGA-P and PLGA-PS was 26.3% and 43.9%, respectively (Table 1). This was also confirmed by gel retardation assay of extracted siRNA from each formulation where it reached 25.7% and 50.7% in PLGA-P and PLGA-PS, respectively (Figure 3). These results indicate a significant increase in siRNA E.E. in PLGA-PS compared to PLGA-P. Similarly, siRNA loading was significantly higher in PLGA-PS compared to PLGA-P reaching $3.8 (\mu\text{g}/\text{mg})$ and $2.2 (\mu\text{g}/\text{mg})$ of PLGA, respectively (Table 1).

3.2. In Vitro Release Profile of siRNA from PLGA-P and PLGA-PS. The cumulative release of siRNA from PLGA-P and PLGA-PS was sustained and followed a triphasic pattern characteristic for PLGA particulate systems

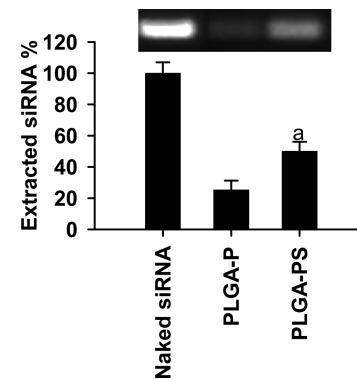


Figure 3. Gel retardation assay of free siRNA and extracted siRNA from PLGA-P and PLGA-PS. The pictures were digitized and analyzed with ImageJ software (W. Rasband (2005) National Institutes of Health, Bethesda, MD, <http://rsb.info.nih.gov/ij>) to determine the mean density of siRNA band. The results are plotted in the bar graph, which represents the average \pm SD of at least 2 tests. Statistical significance (a; $p < 0.05$) compared to PLGA-P.

(Figure 4A). A burst release of siRNA was seen in both PLGA-P and PLGA-PS reaching $\sim 40\%$ in the first 24 h. Thereafter, more sustained and continuous release was observed over a period of 6 days. Then, another climb in

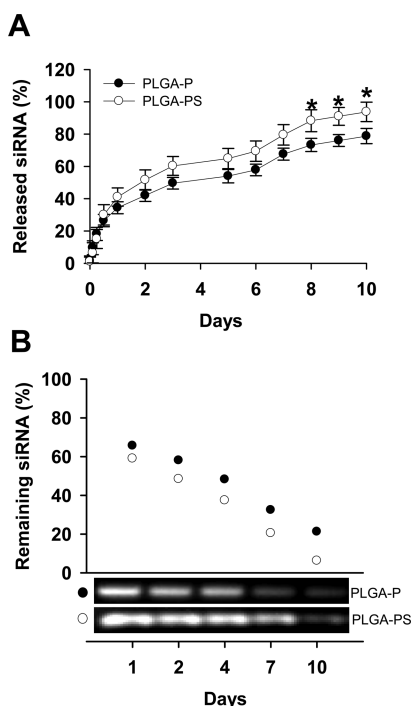


Figure 4. *In vitro* release of siRNA. (A) *In vitro* release profile of FAM-siRNA in PBS detected over 10-day time period for PLGA-P (filled circles) and PLGA-PS (open circles). Significant increase in FAM-siRNA release rate was seen with PLGA-PS at days 8, 9, and 10 compared to PLGA-P (*; $p < 0.05$). Data was presented as average \pm SD of 3 different measurements. (B) Circles represent signals of remaining siRNA extracted from PLGA-P (filled circles) and PLGA-PS (open circles) as determined by gel retardation assay. Percentage of the remaining siRNA in each NPs set was calculated based on extracted siRNA at time 0 for each set. Reduction in entrapped siRNA with time confirms the release profile in (A).

release was seen for both NPs until day 8. At this point, no significant difference in the percentage of siRNA released was observed. By the end of the 10 days, siRNA release was entering a plateau phase where the cumulative release of siRNA was significantly higher for PLGA-PS than that of PLGA-P, reaching almost 94 and 79%, respectively. The analysis of the entrapped siRNA in the NPs was in agreement with the released siRNA: 8% and 24% siRNA was detected in PLGA-PS and PLGA-P, respectively, after 10 days (Figure 4B).

3.3. Assessment of PLGA-P and PLGA-PS Cytotoxicity. In order to assess the cytotoxic effect of PLGA-P and PLGA-PS on DC primary culture compared to PEI and PEI-StA polyplexes that were not encapsulated in PLGA NPs, Trypan Blue assay and MTT assay were conducted to determine cell membrane integrity and metabolic activity, respectively (Figure 5). Only DCs incubated with PLGA-P and PLGA-PS retained their membrane integrity and adequately excluded the Trypan Blue dye. On the contrary, direct application of PEI and PEI-StA polyplexes caused

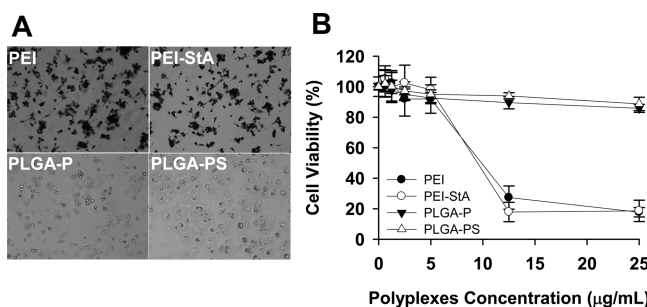


Figure 5. Cytotoxicity assessment of PLGA-P and PLGA-PS compared to PEI and PEI-StA polyplexes. (A) Trypan Blue exclusion test was performed for day 7 DCs treated with 10 $\mu\text{g}/\text{mL}$ of PEI or PEI-StA polyplexes (upper panels) and PLGA-P or PLGA-PS (lower panels). Trypan Blue was detected only with unencapsulated polyplexes, while with PLGA-P and PLGA-PS, DCs were able to exclude the Trypan Blue dye. (B) MTT assay was performed for DCs treated with increasing concentrations of polyplexes before and after PLGA encapsulation. Signs for cytotoxicity started to appear after 5 $\mu\text{g}/\text{mL}$ concentration only with PEI (filled circles) and PEI-StA (open circles). No signs for toxicity were recorded with PLGA-P (filled triangles) and PLGA-PS (open triangles) even at higher concentrations. Data are shown as mean \pm SD of 7 replicates for each sample.

cytoplasmic membrane disruption as evidenced by abundance of the Trypan Blue dye in DCs cytoplasmic compartment (Figure 5A). Furthermore, we conducted a concentration-dependent cytotoxicity study by MTT assay to determine the safety margins of each formulation. As shown in Figure 5B, no cytotoxic effect was noticed at concentrations less than 5 $\mu\text{g}/\text{mL}$ with all formulations. Only after that concentration, reduction in DC viability started to appear with PEI and PEI-StA polyplexes. Moreover, this toxic effect was of a concentration-dependent manner until it reached a plateau after 12.5 $\mu\text{g}/\text{mL}$ concentration. On the other hand, the PLGA-P and PLGA-PS NPs were less toxic than their polyplex counterparts. No significant reduction in cell viability was noted with PLGA-P and PLGA-PS even at higher concentrations.

3.4. Cellular Uptake of PLGA-P and PLGA-PS by DCs. DC primary culture was incubated with PLGA-P and PLGA-PS encapsulating 100 nM siRNA for 6 h at 37 °C. We chose this time point (6 h) as we have previously shown that around 80% of DCs could internalize PLGA NPs within 4–8 h.³³ Our fluorescence microscopy results indicated the presence of the PLGA-P and PLGA-PS of FAM-siRNA (green color in Figure 6, due to FAM-labeled siRNA) in the cytoplasm. Some FAM-siRNA signals were shown to colocalize with Lysotracker Red signals (orange color, due to overlay of the green signal from FAM-siRNA, and the

(33) Elamanchili, P.; Diwan, M.; Cao, M.; Samuel, J. Characterization of poly(D, L-lactic-co-glycolic acid) based nanoparticulate system for enhanced delivery of antigens to dendritic cells. *Vaccine* **2004**, 22 (19), 2406–12.

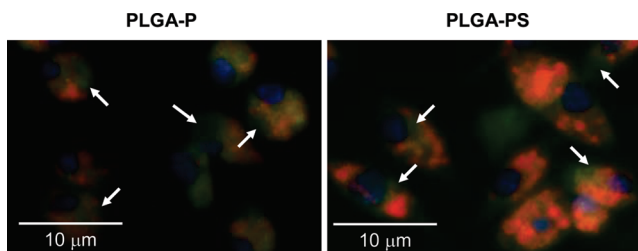


Figure 6. Cellular uptake of FAM-siRNA/PLGA-P and PLGA-PS by DCs. Fluorescence microscopy analysis of intracellular siRNA when DCs were incubated with 100 nM FAM-siRNA/PLGA-P and PLGA-PS (green fluorescence). Colocalization analysis was shown as orange color resulting from an overlay of FAM-siRNA and Lysotracker Red signal. Nuclei (blue) are stained with 4',6-diamidino-2-phenylindole (DAPI), and the scale bar for each image is 10 μ m. White arrows point out siRNA presence in the cytoplasm and perinuclear areas, indicating successful endosomal escape.

red signal from Lysotracker Red), which indicated the presence of PLGA-P and PLGA-PS inside the endosomes and in areas around the nuclei (blue structures, due to DAPI staining). No qualitative differences between the uptake of PLGA-P and PLGA-PS were indicated.

3.5. Restoration of DC Functionality Following STAT3 Knockdown by siRNA NPs. We generated defective and tolerogenic DCs in which the STAT3 phosphorylation has been induced through exposure to conditioned medium of the STAT3-active melanoma cell line B16.F10.³² The STAT3⁺ DCs were then treated with PLGA-P and PLGA-PS of anti-STAT3 siRNA (100 nM) for 48 h. Controls included using naked anti-STAT3 siRNA or identical formulations of scrambled siRNA. We assessed our intervention at four levels: the specific disruption of STAT3 signaling pathway, the induction of phenotypic DC maturation marker (CD86) expression, the induction of proinflammatory cytokine secretion (TNF- α), and the ability of DCs to activate the proliferation of allogenic T cells (Figure 7).

Western blot analysis demonstrated a significant reduction in phosphorylated and total STAT3 signals only by PLGA-P and PLGA-PS NPs of anti-STAT3 siRNA (Figure 7A). Compared to naked siRNA-treated DC group, p-STAT3 level was reduced by ~48% and 77% upon treatment with PLGA-P and PLGA-PS, respectively. More importantly, the noted inhibition in p-STAT3 level was specific since it was correlated with reduction in total STAT3 level as a result of siRNA silencing. Furthermore, PLGA-PS allowed for more profound siRNA silencing of STAT3 that was statistically significant compared to PLGA-P ($p < 0.05$). No silencing effect was noticed with scrambled siRNA formulations (PLGA-P-sc or PLGA-PS-sc) indicating the specificity of our intervention.

The induction of p-STAT3 in DCs by B16-CM reduced their phenotypic maturation as we have previously demonstrated.³² The siRNA silencing of STAT3 in DCs restored surface expression of DC maturation marker CD86. As

shown in Figure 7B, DC groups treated with PLGA-P and PLGA-PS expressed remarkably high levels of CD86. The mean fluorescence intensity (MFI) of the FACS histograms was 93 and 111 for cells treated with PLGA-P and PLGA-PS, respectively, as compared to only 33 in the case of naked siRNA-treated DCs (Figure 7B). Scrambled siRNA formulations (PLGA-P-sc or PLGA-PS-sc) did not induce CD86 expression, which is in agreement with our Western blot results (data in Figure 7A).

This maturation picture was accompanied by a significant induction in TNF- α secretion by DCs treated with PLGA-P or PLGA-PS (Figure 7C). DCs treated with PLGA-P were shown to secrete TNF- α at levels that were 3.4-fold higher than what was recorded with naked siRNA-treated group. Treatment of DCs with PLGA-PS has led to the secretion of TNF- α at 5.7-fold higher than naked siRNA control treatment. In fact, TNF- α secretion upon treatment with PLGA-PS was even 1.7-fold higher than what followed PLGA-P treatment. This was consistent with our FACS analysis findings where CD86 expression was induced only after treatment with PLGA-P and, particularly, after treatment with PLGA-PS.

More importantly, this immunostimulatory picture was corroborated by the ability of DCs to induce allogenic T cells proliferation (Figure 7D). DCs treated with naked siRNA or PLGA-P-sc or PLGA-PS-sc were not able to interact with allogenic T cells. However, PLGA-P or PLGA-PS that deliver functional anti-STAT3 siRNA allowed DCs to significantly induce allogenic T cell proliferation. A 4.4- and 5.6-fold increase in the proliferation of T cells cocultured with DCs treated with PLGA-P or PLGA-PS was observed, respectively (Figure 7D).

4. Discussion

In a variety of solid and hematological tumors, constitutive activation of STAT3 has been found to mediate numerous oncogenic properties such as cancer cell survival, proliferation, angiogenesis, metastasis, and immune escape.^{34–36} The latter is centrally driven by tumor-mediated inhibition of DC maturation.^{8,14} For optimum immune response, mDCs must provide T cells with three signals: signal 1, which represents the antigen presentation in context of class I and class II MHC; signal 2, which is the costimulation provided by surface molecules such as CD80, CD86, and CD40 that interact with their ligands on T cell surface; and signal 3, which is the set of cytokines released by mDCs that polarizes T cells toward the intended response. Failure of DCs to

- (34) Buettner, R.; Mora, L. B.; Jove, R. Activated STAT Signaling in Human Tumors Provides Novel Molecular Targets for Therapeutic Intervention. *Clin. Cancer Res.* **2002**, *8*, 945–954.
- (35) Hirano, T.; Ishihara, K.; Hibi, M. Roles of STAT3 in mediating the cell growth, differentiation and survival signals relayed through the IL-6 family of cytokine receptors. *Oncogene* **2000**, *19* (21), 2548–56.
- (36) Yu, H.; Pardoll, D.; Jove, R. STATs in cancer inflammation and immunity: a leading role for STAT3. *Nat. Rev. Cancer* **2009**, *9* (11), 798–809.

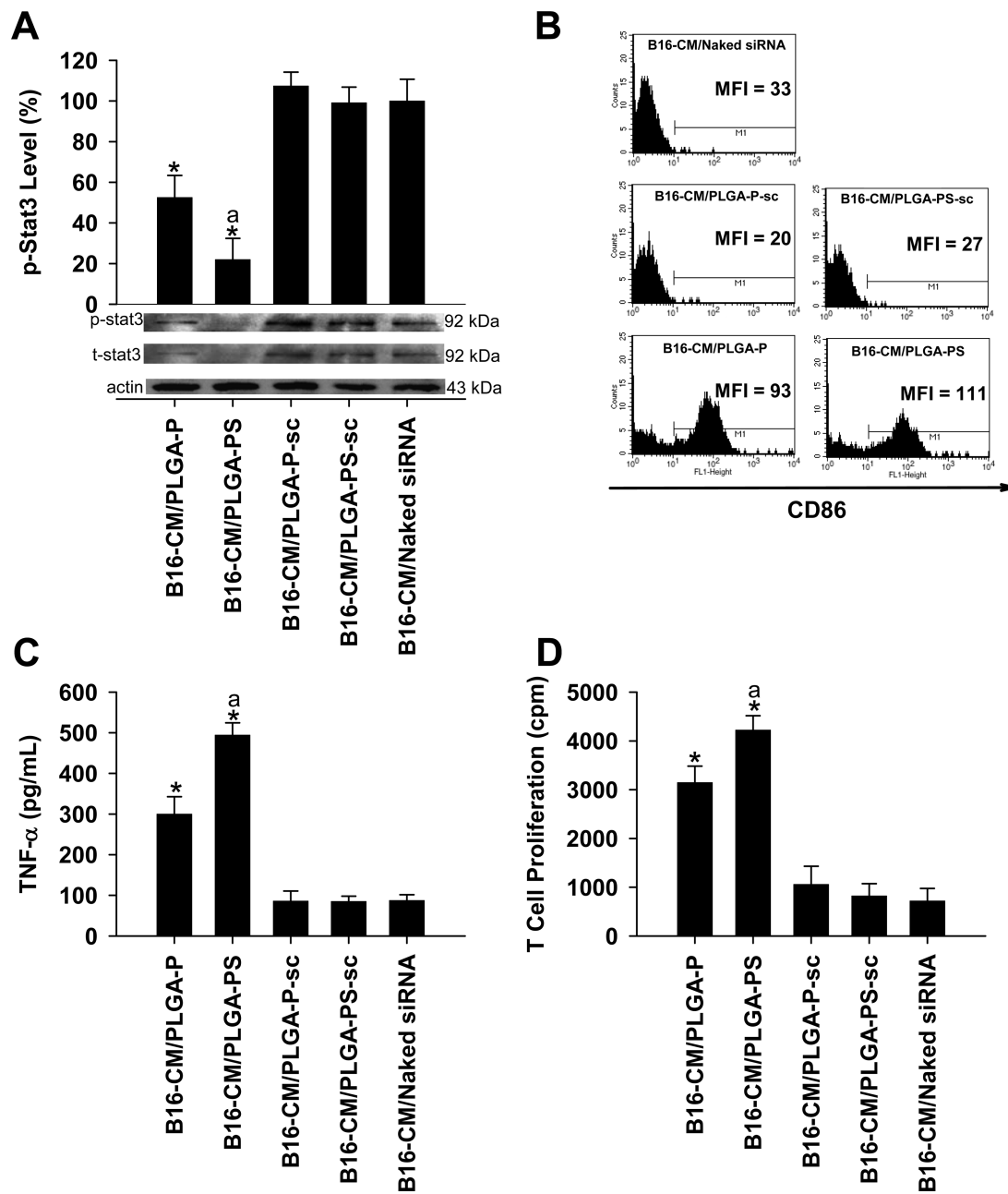


Figure 7. Evaluation of immunostimulatory potential of PLGA-P and PLGA-PS of STAT3 siRNA. Primary DC cultures in day 7 were incubated with B16-CM of B16 culture for 24 h. DCs were pulsed with anti-STAT3 PLGA-P and PLGA-PS for 48 h. (A) Western blot analysis showing expression level of p-STAT3, STAT3, and actin loading control. Bands optical intensities of p-STAT3 (black bars) were quantified and normalized to actin bands using ImageJ software (W. Rasband (2005) National Institutes of Health, Bethesda, MD, <http://rsb.info.nih.gov/ij>). The software provides optical densities that are normalized for width, thickness, and background. Data are shown as the average \pm SD of 4 experiments. Statistical significance was determined compared to control (*; $p < 0.05$) and PLGA-P (a; $p < 0.05$). (B) FACS analysis of CD86 expression. Histograms indicate a shift in the fluorescence signal only following STAT3 knockdown in DCs. Mean fluorescence intensity (MFI) values after each treatment were reported for M1 population. M1 gate region indicates the inclusion area for CD86 expression where in-gate cells are considered positive for marker expression. (C) TNF- α cytokine levels measured in DC culture following STAT3 knockdown. Significant induction TNF- α cytokine secretion was noted with PLGA-PS compared to control groups (*; $p < 0.05$) and PLGA-P group (a; $p < 0.05$). Data are shown as the average \pm SD of 3 measurements. (D) Allogenic MLR following STAT3 silencing *in vitro*. Treated DCs were collected, irradiated, and cocultured with allogenic T cells isolated from the spleen of Balb/c mouse. Bars represent level of T cell proliferation. DCs treated with PLGA-PS allowed for higher alloreactivity compared to controls (*; $p < 0.05$) and PLGA-P (a; $p < 0.05$).

conduct these stimulatory signals leads to a state of immune tolerance where T cells become inactive.³⁷ In fact, robust antitumor immune response is governed by the capacity of mDCs to polarize T cells toward Th1/CTL response.^{14,38} However, tumors tend to escape immune recognition and response by abrogating DC activation via p-STAT3 induction.⁸ This immunosuppressive/regulatory effect, caused by tumors, imposes a state of immunological paralysis and potentiates cancer progression.³⁹ Therefore, inhibition of STAT3 signal in tumor-exposed DCs was shown to be of critical significance to break tumor-mediated immune tolerance and induce robust antitumor immune response.¹⁶

Efficient inhibition of STAT3 signaling pathway in DCs was sought by the employment of various modalities such as pharmacological inhibition by AG490 and JSI-124.^{17,40} However, this approach is not suitable for clinical practice due to the nonspecific nature of these agents.²² The inhibitory effect of AG490 on JAK/STAT3 pathway has been recently shown to be through the inhibition of gp130 expression, which is the signaling chain in IL-6 receptor complex at which JAK docks to phosphorylate STAT3.⁴¹ Other members of the IL-6 family, namely, cardiotrophin 1 (CT-1), leukemia inhibitory factor (LIF), ciliary neurotrophic factor (CNTF), oncostatin M (OSM), and IL-11, depend on gp130 for signal transduction.⁴² Therefore, the loss of gp130 basically eliminates multiple physiologically-critical events. Similarly, JSI-124 was shown to profoundly affect the actin cytoskeleton via STAT3-independent mechanism at effective JAK2/STAT3 inhibitory concentration in both cancerous and noncancerous cells.⁴⁰ This nonspecific action may highly account for the JSI-124 cytotoxic effect. We have previously shown that PLGA NPs of chemically-conjugated JSI-124 can indeed reduce p-STAT3 level in B16-CM-exposed-DCs, and mitigate the deleterious effect of JSI-124.⁴³ Although the study provided important proof-of-concept results, we were interested in investigating a more clinically relevant strategy.

- (37) Mueller, D. L. Mechanisms maintaining peripheral tolerance. *Nat. Immunol.* **2010**, *11* (1), 21–7.
- (38) Knutson, K. L.; Disis, M. L. Tumor antigen-specific T helper cells in cancer immunity and immunotherapy. *Cancer Immunol. Immunother.* **2005**, *54* (8), 721–8.
- (39) Chaput, N.; Conforti, R.; Viaud, S.; Spatz, A.; Zitvogel, L. The Janus face of dendritic cells in cancer. *Oncogene* **2008**, *27* (45), 5920–31.
- (40) Graness, A.; Poli, V.; Goppelt-Struebe, M. STAT3-independent inhibition of lysophosphatidic acid-mediated upregulation of connective tissue growth factor (CTGF) by cucurbitacin I. *Biochem. Pharmacol.* **2006**, *72* (1), 32–41.
- (41) Seo, I. A.; Lee, H. K.; Shin, Y. K.; Lee, S. H.; Seo, S. Y.; Park, J. W.; Park, H. T. Janus Kinase 2 Inhibitor AG490 Inhibits the STAT3 Signaling Pathway by Suppressing Protein Translation of gp130. *Korean J. Physiol. Pharmacol.* **2009**, *13* (2), 131–8.
- (42) Kishimoto, T.; Akira, S.; Narazaki, M.; Taga, T. Interleukin-6 family of cytokines and gp130. *Blood* **1995**, *86* (4), 1243–54.
- (43) Molavi, O.; Mahmud, A.; Hamdy, S.; Hung, R.; Samuel, J.; Lai, R.; Lavasanifar, A. Development of a poly(D,L-lactic-co-glycolic acid) (PLGA) nanoparticle formulation of STAT3 inhibitor JSI-124: Implication for cancer immunotherapy. *Mol. Pharmaceutics* **2010**, *7* (2), 364–74.

Therefore, we employed anti-STAT3 siRNA as a specific modality for STAT3 inhibition in B16-CM-exposed DCs.

We were able to load precomplexed siRNA with PEI and PEI-StA in PLGA NPs, i.e., PLGA-P and PLGA-PS, respectively. Characterization of PLGA-P and PLGA-PS for surface morphology demonstrated the formation of nanospheres of smooth surface and in a size range comparable to the hydrodynamic diameter measured by DLS that showed unimodal distributions for all NPs (Figure 2). Furthermore, despite the known cationic charge of PEI, the anionic surface charge seen on the PLGA-P and PLGA-PS surface could mostly be a covering effect due to the anionic density of the carboxylic-acid-terminated PLGA. Masking the dense cationic charge in PLGA NPs may be the reason behind the significant reduction in the nonspecific toxicity of PEI and PEI-StA polyplexes toward DCs when incorporated in PLGA NPs (Figure 5). The E.E. and loading of siRNA by PLGA-PS was significantly higher than that of PLGA-P (Table 1). This observation can be attributed to the intrinsically higher binding capacity of PEI-StA toward siRNA as compared to PEI.²⁷

The release profile indicates that complete siRNA release is dependent on PLGA NP degradation (Figure 4A). Moreover, the noted 40% burst release is mainly due to presence of siRNA polyplexes on or near the surfaces of PLGA NPs. Furthermore, since PEI and PEI-StA are relatively more hydrophilic compared to PLGA, they may induce formation of aqueous channels in the PLGA matrix.^{44,45} The channels could then serve as outlets for siRNA diffusion. Such an effect was reported with the release of oligonucleotides from PEI-containing PLGA microspheres, which was correlated with the amount of PEI added to the aqueous phase.⁴⁴ Others have also reported a similar pattern of siRNA release from PLGA NPs that incorporates PEI.⁴⁵ We also noticed that siRNA release from PLGA-PS becomes faster than its release from PLGA-P, especially at the end of the release profile (Figure 4A). The reason behind this could be the higher electrostatic interaction between PEI polyplexes and PLGA than that of PEI-StA, which drives PEI polyplexes to remain attached to the PLGA matrix. This is an important observation as it implies that we can control the release of siRNA by modifying the structure of the polyplexes. The faster release of siRNA from PLGA-PS may also be attributed to the higher loading of PEI-StA compared to PEI polyplexes in PLGA NPs.

PLGA-P and PLGA-PS were found nontoxic to DCs compared to the cationic polyplexes alone (Figure 5). We attribute the significant reduction in PEI toxicity after

-
- (44) De Rosa, G.; Quaglia, F.; La Rotonda, M. I.; Appel, M.; Alphandary, H.; Fattal, E. Poly(lactide-co-glycolide) microspheres for the controlled release of oligonucleotide/polyethylenimine complexes. *J. Pharm. Sci.* **2002**, *91* (3), 790–9.
 - (45) Patil, Y. B.; Swaminathan, S. K.; Sadhukha, T.; Ma, L.; Panyam, J. The use of nanoparticle-mediated targeted gene silencing and drug delivery to overcome tumor drug resistance. *Biomaterials* **2010**, *31* (2), 358–65.

incorporation into PLGA NPs to two factors: (i) participation of PLGA in preventing the surface exposure of the cationic charge as evidenced by our zeta potential analysis (Figure 2B), thus prevention of PEI-induced membrane disintegration, and (ii) the intrinsic safety of PLGA NPs since PLGA is an FDA-approved biodegradable polymer that had been widely used in several controlled-release drug products for human use and as a delivery system for DC.^{46,47} Although it is arguable that the sustained release effect dictated by the PLGA system may lower PEI toxicity below detection by reducing the exposure rate of PEI to the cells, we do not anticipate this profile to be the reason behind the noticed mitigation in PEI toxicity. In fact, the *in vitro* release pattern might not be exactly mirrored after cellular internalization where the NPs are exposed to variable pH ranges in different intracellular compartments, which would influence the release pattern. We argue that the considerable concealment of the cationic charge within the PLGA particles and the unique ability of PLGA NPs for endosomal escape (discussed below) could prevent membrane disintegration and the release of the cytotoxic lysosomal contents into the cytoplasm. Additionally, the improvement of PEI toxicity profile by incorporation into PLGA system has been also shown in other cell types indicating the reliability of the approach.²⁹ Moreover, it has been documented that PLGA particles did not significantly affect the viability of DCs even when DCs were loaded with large number of PLGA particles and even during PLGA degradation where acidic byproducts are formed.⁴⁸

The constructed NPs were successfully internalized by DCs (Figure 6). The fact that these particles fit in the preferable size for DC endocytosis (Figure 2) is one reason for the high intracellular signal.³³ Moreover, it has been argued that the presence of PEI in the polymeric matrix of PLGA facilitates cellular uptake and enhances the transfection efficiency to some extent.²⁹ Nonetheless, since the uptake study was performed on pure DC culture, it is hard to estimate the effectiveness of these NPs in preferentially targeting DCs. Determination of NP uptake by DCs in the presence of other cells or *in vivo* studies is needed for clearer and more conclusive assessment. Our localization studies confirm the presence of our formulations in the endosomal compartments as indicated by the orange color resulting from the colocalization of FAM-siRNA/PLGA-P and PLGA-PS with the Lysotracker Red. Moreover, green fluorescence of siRNA was also detected in the cytoplasmic compartment, which is indicative of an endosomal escape property of the

- (46) Bala, I.; Hariharan, S.; Kumar, M. N. PLGA nanoparticles in drug delivery: the state of the art. *Crit. Rev. Ther. Drug Carrier Syst.* **2004**, *21* (5), 387–422.
- (47) Waeckerle-Men, Y.; Groettrup, M. PLGA microspheres for improved antigen delivery to dendritic cells as cellular vaccines. *Adv. Drug Delivery Rev.* **2005**, *57* (3), 475–82.
- (48) Walter, E.; Dreher, D.; Kok, M.; Thiele, L.; Kiama, S. G.; Gehr, P.; Merkle, H. P. Hydrophilic poly(DL-lactide-co-glycolide) microspheres for the delivery of DNA to human-derived macrophages and dendritic cells. *J. Controlled Release* **2001**, *76* (1–2), 149–68.

particulate systems. A combination of two phenomena might be responsible for this property: (i) proton-sponge effect provided by the PEI system, and (ii) surface cationization of PLGA NPs in the acidic pH of secondary endosomes.⁴⁹ The latter was also confirmed in PLGA NPs internalized by DCs, where endosomal escape mediated cross-presentation of exogenous antigens.⁵⁰ Surface cationization of PLGA in acidic pH was attributed to the transfer of excess protons from the bulk liquid to the NP surface or attributed to hydrogen bonding between carboxyl groups of PLGA and hydronium molecules in the acidic pH.^{49,51}

The results of cell culture study indicate the following: (i) Phenotypical and functional maturation of B16-CM-exposed DCs can be restored, *in vitro*, after DC incubation with anti-STAT3 siRNA PLGA-P and PLGA-PS. (ii) The level of DC activation is correlated with the level of STAT3 knockdown (Figure 7A). We show that DC alloreactivity (Figure 7D) was noticed only following STAT3 knockdown and the induction of the costimulatory molecule expression CD86 (Figure 7A and 7B). This is an important observation since it proves that siRNA was successfully unpacked at the site of action and encountered its cytoplasmic target. The CD86 on DC surface is known to interact with CD28. In turn, T cells provide stimulatory signal to DCs via CD40/CD40-ligand (CD40L) interaction. Such interaction is beneficial for both DCs and T cells where stimulation of CD28 stabilizes CD40L on T cells and stimulation of CD40 on DCs increases their expression of CD86 molecules.^{52,53} Moreover, the remarkable secretion of the proinflammatory cytokine TNF- α from DCs upon STAT3 knockdown provides additional evidence of restoring DC function. When secreted by activated DCs, TNF- α was demonstrated to induce T cell activation and polarize T cells toward Th1/CTL response.^{54,55} We attribute the collective picture of DC activation to STAT3 knockdown by siRNA and not merely

-
- (49) Panyam, J.; Zhou, W. Z.; Prabha, S.; Sahoo, S. K.; Labhasetwar, V. Rapid endo-lysosomal escape of poly(DL-lactide-co-glycolide) nanoparticles: implications for drug and gene delivery. *FASEB J.* **2002**, *16* (10), 1217–26.
 - (50) Shen, H.; Ackerman, A. L.; Cody, V.; Giodini, A.; Hinson, E. R.; Cresswell, P.; Edelson, R. L.; Saltzman, W. M.; Hanlon, D. J. Enhanced and prolonged cross-presentation following endosomal escape of exogenous antigens encapsulated in biodegradable nanoparticles. *Immunology* **2006**, *117* (1), 78–88.
 - (51) Makino, K.; Ohshima, H.; Kondo, T. Transfer of protons from bulk solution to the surface of poly(L-lactide) microcapsules. *J. Microencapsulation* **1986**, *3* (3), 195–202.
 - (52) Johnson-Leger, C.; Christensen, J.; Klaus, G. G. CD28 co-stimulation stabilizes the expression of the CD40 ligand on T cells. *Int. Immunol.* **1998**, *10* (8), 1083–91.
 - (53) Yang, Y.; Wilson, J. M. CD40 ligand-dependent T cell activation: requirement of B7-CD28 signaling through CD40. *Science* **1996**, *273* (5283), 1862–4.
 - (54) Brunner, C.; Seiderer, J.; Schlamp, A.; Bidlingmaier, M.; Eigler, A.; Haimerl, W.; Lehr, H. A.; Krieg, A. M.; Hartmann, G.; Endres, S. Enhanced dendritic cell maturation by TNF-alpha or cytidine-phosphate-guanosine DNA drives T cell activation *in vitro* and therapeutic anti-tumor immune responses *in vivo*. *J. Immunol.* **2000**, *165* (11), 6278–86.

to NP uptake by DCs. Endocytosis-induced DC maturation is debatable in literature, and evidence that either confirms⁵⁶ or contradicts^{49,57} this notion has been documented with PLGA NPs. We take the latter position since our study showed no effect of scrambled-siRNA NPs (PLGA-P-sc or PLGA-PS-sc) in restoring DC maturation, which strongly supports the specificity of our approach where STAT3 knockdown is required for the observed effect. In fact, STAT3 inhibition in DCs was associated with the maturation process even without tumor exposure.¹⁷ Furthermore, the superior effect of PLGA-PS over PLGA-P in mediating siRNA silencing is most likely due to the ability of PEI-StA to protect siRNA from nuclease degradation to higher extent than PEI as we have previously demonstrated.²⁷ However, using the proposed approach, *in vivo* studies for siRNA-

mediated STAT3 knockdown in DCs are needed now to better evaluate the therapeutic potential of this formulation.

5. Conclusion

We have developed a PLGA-based delivery system of siRNA by the aid of PEI and PEI-StA for STAT3 knockdown in DCs *in vitro*. The formulation successfully mediated specific siRNA silencing with no signs of nonspecific toxicities. Moreover, this approach was successful in restoring DC function that had been compromised by the exposure to B16-CM. This strategy, if proven successful *in vivo*, holds promise for inclusion with other immunotherapeutic strategies such as cancer vaccine and adjuvant therapy, and opens a window for *ex vivo* manipulation of DCs for therapeutic purposes.

- (55) Mariotti, S.; Sargentini, V.; Marcantonio, C.; Todero, E.; Teloni, R.; Gagliardi, M. C.; Ciccarello, A. R.; Nisini, R. T-cell-mediated and antigen-dependent differentiation of human monocyte into different dendritic cell subsets: a feedback control of Th1/Th2 responses. *FASEB J.* **2008**, 22 (9), 3370–9.
- (56) Yoshida, M.; Babensee, J. E. Molecular aspects of microparticle phagocytosis by dendritic cells. *J. Biomater. Sci., Polym Ed* **2006**, 17 (8), 893–907.
- (57) Waeckerle-Men, Y.; Scandella, E.; Uetz-Von Allmen, E.; Ludewig, B.; Gillessen, S.; Merkle, H. P.; Gander, B.; Groettrup, M. Phenotype and functional analysis of human monocyte-derived dendritic cells loaded with biodegradable poly(lactide-co-glycolide) microspheres for immunotherapy. *J. Immunol. Methods* **2004**, 287 (1–2), 109–24.

Acknowledgment. This project was funded by operating grants to J.S. and A.L. from the Canadian Institute of Health Research (MOP 42407) and to H.U. from CIHR (MOP 74452) and NSERC. A.A. is sponsored by an active scholarship from King Saud University, Riyadh, Saudi Arabia. B16.F10 cell line was kindly provided by Dr. Mavanur Suresh, University of Alberta. Mrs. Vanessa Incani is highly thanked for synthesizing PEI-StA. Technical help of SEM facility staff is acknowledged, University of Alberta. Technical help of flow cytometry facility staff is acknowledged, Cross Cancer Institute, Edmonton, AB, Canada.

MP100067U